IEEE Access
Multidisciplinary ⋮ Rapid Review ⋮ Open Access Journal

Received 30 September 2025, accepted 9 November 2025, date of publication 12 November 2025,
date of current version 21 November 2025.

Digital Object Identifier 10.1109/ACCESS.2025.3631947

RESEARCH ARTICLE

Intelligent Proximity Correction Enabled Large-Area Metasurfaces by KrF Photolithography

HSUEH-LI LIU[1], SHENG-HSIANG SU[1], PO-KAI CHANG[1], YOU-CHIA CHANG[1], YAO-WEI HUANG[1], (Member, IEEE), CHIA-WEI CHANG[2], TSAI-MING HUANG[2], CHUN-CHI CHEN[2], WEN-HSIEN HUANG[2], JIA-MIN SHIEH[1,2], AND PEICHEN YU[1], (Member, IEEE)

[1]Department of Photonics, College of Electrical and Computer Engineering, National Yang Ming Chiao Tung University, Hsinchu 30010, Taiwan
[2]Taiwan Semiconductor Research Institute, National Institutes of Applied Research, Taipei 106214, Taiwan

Corresponding author: Peichen Yu (peichen.yu@nycu.edu.tw)

This work was supported in part by the National Science and Technology Council, Taiwan, under Grant NSTC113-2640-E-A49 -002 and Grant NSTC112-2221-E-A49 -065 -MY3

ABSTRACT Model-based optical proximity correction (OPC) is a widely adopted resolution enhancement technique that compensates for lithography proximity effects by adjusting and correcting mask pattern shapes. However, its application to large-area, high-density patterns such as metasurfaces is constrained by the computational demands of image calculation in the lithographic model. This paper introduces an intelligent proximity correction (IPC) system that leverages a deep-learning U-net-based lithographic model to optimize mask designs through iterative algorithms. By eliminating the need for optical calculations while maintaining accurate predictions of photoresist contours directly from mask patterns, the intelligent lithography model demonstrated a 3-fold reduction in simulation time compared to conventional optical models. Overall the IPC system with parallel computation achieves a remarkable 35-fold speed increase compared to conventional OPC approaches without compromising correction accuracy. Experimental results demonstrate that IPC is effective in fabricating high-efficiency, large-area metalenses and metasurface holograms for the visible wavelength using KrF photolithography, opening possibilities to produce complex, large-scale metasurfaces for various applications in optics and photonics.

INDEX TERMS Metasurface, photolithography, optical proximity correction, deep-learning, U-net.

I. INTRODUCTION

Metasurfaces have emerged as a revolutionary technology in optics, offering abilities to manipulate light with unprecedented control using subwavelength structures [1], [2], [3], [4], [5]. These flat optical components aim to replace bulky, conventional optical elements with ultra-thin, lightweight alternatives that can be mass-produced using standard semiconductor fabrication techniques [6], [7], [8], [9]. However, realizing large-area, high-performance metasurfaces using economical photolithography techniques such as i-line steppers or KrF scanners remains challenging due to lithographic proximity effect [10], [11]. Optical proximity correction (OPC) that can mitigate diffraction effects and improve pattern fidelity by adjusting mask pattern shapes has been widely adopted in semiconductor industry [12], [13]. However, conventional OPC methods require complex optical image calculation due to partially coherent illumination systems, which have become prohibitively time-consuming and computationally expensive for large-area, high-density patterns such as metasurfaces [14], [15].

Recent advancements in deep learning have opened new avenues for enhancing lithographic processes [16], [17], [18], [19]. In particular, the application of neural networks to model and predict end patterns from the initial design has shown promise in improving both accuracy and computational efficiency [20], [21], [22], [23]. Building on these developments, this paper introduces an intelligent proximity

The associate editor coordinating the review of this manuscript and approving it for publication was Qi Luo.

correction (IPC) system that leverages deep-learning neural networks to enable the fabrication of high efficiency and large-area metalens and metasurfaces in the visible wavelength range using KrF photolithography.

Our IPC system utilizes a U-net–based lithographic surrogate embedded directly into the iterative correction loop, rather than serving only as a forward predictor as in prior ML studies. By removing the need for conventional optical simulations while still providing accurate photoresist contour predictions, the system achieves 3× faster convergence compared to our previous optical model [24], and ∼35× faster than conventional OPC without parallelization, all while preserving pattern fidelity. This approach allows for the correction of much larger metasurface designs within practical timeframes, opening the door to fabricating large-area, high-performance metasurfaces using economical exposure systems.

In this paper, we first describe the development and implementation of our IPC system and its integration with KrF photolithography. We then demonstrate the system efficacy through the fabrication of metasurface holograms and metalenses, validating both design fidelity and large-area scalability. A detailed comparison with a previously reported OPC technique is presented, showing that the proposed IPC approach achieves substantial improvements in correction speed, accuracy, and practicality for wafer-scale metasurface manufacturing.

II. EXPERIMENTAL METHOD

A. THE IPC SYSTEM

The workflow of the IPC system is illustrated in Figure 1(a), showing the iterative process of refining photomask designs for improved pattern fidelity. The process begins with an initial mask pattern, processed through a neural-network-based lithographic model to simulate the developed photoresist patterns, namely, the resist image. This resist image is then compared to the desired target pattern to evaluate the differences of contour positions at the evaluation points, which is called the edge placement error (EPE). If a mismatch is identified, the system adjusts the mask boundaries accordingly to minimize the EPE for all evaluation points. These adjustments continue until the resist image closely matches the target pattern. The program terminates when the average EPE falls below one pixel.

The IPC system employs a U-net neural network for lithographic pattern transfer modeling [25], [26], as illustrated in Figure 1(b). The network architecture comprises an encoder-decoder framework that maps input photomask patterns to their corresponding photoresist outcomes following exposure and development processes. The encoder pathway consists of cascaded convolutional layers integrated with the max pooling operations and rectified linear unit (ReLU) activation functions. This configuration enables hierarchical feature extraction while progressively reducing spatial dimensions. The decoder pathway employs up-sampling operations with convolutional and ReLU layers to reconstruct the output dimensions. Skip connections between corresponding encoder and decoder layers facilitate the integration of multi-scale features, thereby enabling precise reconstruction of photoresist patterns. The detailed U-net model architecture can be found in the supporting information (Table S1).

The model training and validation processes involve using an experimental dataset comprising 5152 pairs of photomask and photoresist patterns. Photoresist patterns were acquired via scanning electron microscopy (SEM) at 4k resolution (4096 × 3775 pixels). Subsequently, the images were partitioned into 512 pixel ×512 pixel segments. Data augmentation via translation and rotation operations yields the final dataset of 5152 image pairs. The dataset was subdivided with 3864 pairs (75%) allocated to training and 1288 pairs (25%) to validation. Before network input, all images underwent normalization to the range [0, 1]. Network training was executed with a batch size 32, constrained by available GPU memory capacity. The training process continued for 500, 1000, 1500, and 2000 epochs respectively to achieve convergence, where the mean square error (MSE) was used as the model loss function.

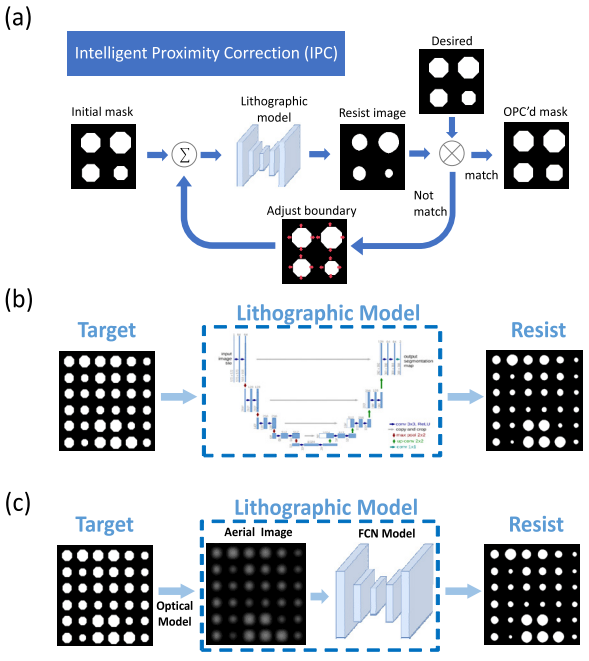

FIGURE 1. (a) The proposed intelligent proximity correction (IPC) system. (b) The IPC lithographic model structure. (c) The OPC lithographic model incorporates the optical aerial image calculation and a fully convolutional network (FCN) resist model.

The performance of the proposed IPC system is benchmarked against our in-house OPC method using the lithographic model detailed in [24], where the litho-model performs the photomask to photoresist transformation through two stages: optical simulation and photoresist modeling (Fig. 1(c)). The optical stage calculates the optical intensity distribution on the wafer, known as the aerial image,

using Hopkin's formulation. The photoresist stage then uses a fully convolutional network (FCN) to learn the photoresist behavior in response to the aerial image. The detailed FCN model architecture is provided in the supporting information (Table S2). We refer to this lithographic model as the FCN model hereafter. For a fair comparison, the FCN model exploits the same dataset as the U-net model. The photomask images are convoluted with the optical kernels corresponding to the KrF scanner settings to prepare the aerial image and resist image pairs for training and validation. Table 1 compares the FCN and U-Net models in terms of parameter counts, prediction time, and memory usage for a 4096 × 4096 pixel tile. Benchmarks were performed on a 12th Gen Intel® Core™ i9-12900K @ 3.20 GHz, 16-core, x64 workstation. The U-Net model achieves substantially lower prediction time and memory usage compared to the FCN baseline.

TABLE 1. Comparison of FCN and U-Net models for lithographic modeling.

Model	FCN	U-net
Parameter Counts	85097	123125
Pixels per tile	4096 x 4096	4096 x 4096
Predict time (s)	9.39	0.95
Memory (MB)	451.29	17.54
Processor	12th Gen Intel® Core™ i9-12900K @ 3.20GHz ; X64 ; Core 16	

The well-trained lithography model is integrated into the IPC system for fast and accurate photomask correction. The IPC system first divides a large input photomask pattern into main tiles of 3584 × 3584 pixels. To mitigate stitching errors, each main region is appended with a 512-pixel ambient margin, resulting in an IPC template size of 4096 × 4096 pixels. This ambient overlap ensures that stitching artifacts are effectively suppressed when the corrected main tiles are reassembled. A message passing interface- (MPI) based framework distributes these tiles in parallel to the processing nodes of a supercomputer. On each node, the U-net model predicts the printed photoresist pattern corresponding to the mask tile and feedback to the correction algorithm to adjust the mask tile accordingly. Once all tiles are corrected, the main region of all tiles are stitched back to reconstruct the fully optimized mask pattern. The IPC system employs 11 computing nodes from Taiwania-3, allowing a 2 mm diameter metalens mask to be corrected within 2.5 hour compared to weeks for the previous OPC framework. The combination of simulation speedups from ML-based lithography models with parallel processing of mask optimization in IPC provides a promising avenue to unlock economical nano-fabrication capabilities for large-scale metasurfaces.

B. METASURFACE DESIGN AND FABRICATION

The metasurfaces comprise silicon nitrides (SiN_x) nano-cylinder arrays fabricated on 0.7 mm thick glass wafers. Each nano-cylinder functions as an antenna, imparting an engineered phase shift within a square lattice arrangement. At the operating wavelength of 532 nm, the PECVD SiN_x used in this study has a refractive index (n) of 2.17 and an extinction coefficient (k) of 0.000998. Using commercial rigorous coupled-wave analysis (RCWA) implementation, we simulated the transmittance and phase shifts of electromagnetic fields passing through nano-cylinders with varying diameters and heights (Fig. 2(a) and 2(b)). The final design employs nano-cylinders with diameters ranging from 100-256 nm, a 457 nm pitch, and 585 nm height for 532 nm wavelength operation, achieving high transmission and nearly complete 2π phase coverage (Fig. 2(c)). This cell library enables the design of various metasurfaces, including focusing lenses and phase-only computer-generated holograms (CGHs) though the local periodic approximation (LPA). This approximation is generally valid when the nanopillar geometry and filling ratio vary gradually across the device. Under these conditions, each pillar can be treated as imparting a local phase delay through its effective mode profile, while inter-pillar coupling effects remain limited [27]. Prior studies have reported good agreement between LPA predictions and full-wave Maxwell solvers even for rapidly varying aperiodic patterns [28].

Here, we demonstrate ideal metalens designs with 0.1 numerical aperture (NA) and various lens diameters. The focusing profile from a scaled 40 μm-diameter metalens calculated using finite difference time domain (FDTD) followed by beam propagation method (BPM) for free space propagation. The simulated focal length was 191 μm with 64.0% absolute focusing efficiency (Fig. 2(d)). For CGH designs to project customized patterns in the far field, we implemented a modified Gerchberg-Saxton (GS) algorithm, which incorporates gradient descent optimization of intensity error to iteratively refine the phase estimation to meet the design target [29], [30], [31].

The metalens and metasurface devices are fabricated through KrF photolithography with a 6-inch chrome-on-glass binary mask at the Taiwan Semiconductor Research Institute (TSRI). The process began with an 8-inch glass wafer coated with 500 nm aluminum (Al) and silicon oxides (SiO_x) layers on the rear for glass wafer registration and protection respectively. A 585 nm thick SiN_x layer was deposited via Plasma Enhanced Chemical Vapor Deposition (PECVD) on the front, followed by a 120 nm tantalum (Ta) layer as the etch mask via Physical Vapor Deposition (PVD). Using a Tokyo Electron TRACK-ACT8 system, a back anti-reflection coating (BARC) and photoresist (CARD, GKR-5201A) were spin-coated and soft-baked. The pattern was exposed using a Canon FPA-6300ES6a

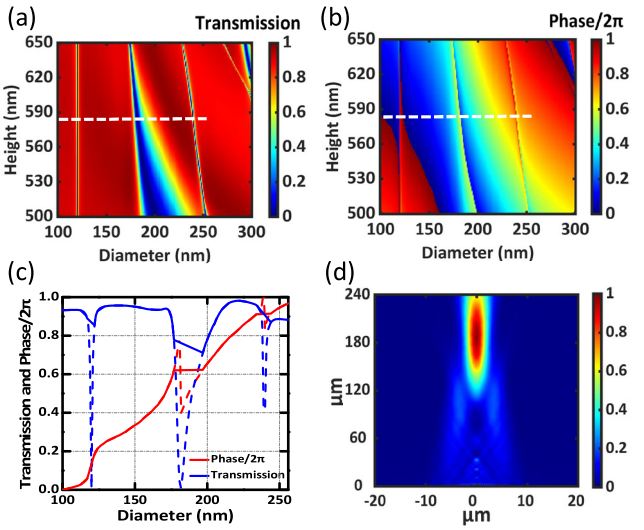

FIGURE 2. Design of metalens and metasurface hologram for the 532 nm wavelength. The simulated (a) transmission and (b) phase map as a function of the nano-cylinder heights and diameters at the 457 nm pitch. (c) The transmission and phase of the chosen cell library with a square lattice arrangement, where the height is 585 nm the diameters varying between 120 nm to 256 nm. (d) The simulated focusing profile of a scaled metalens design with NA=0.1 from cell library in (c). The diameter is 40 μm and the simulated focal length results is 191 μm.

KrF DUV scanner, followed by post-exposure bake (120°C, 90s), development, and hard bake (110°C, 60s). The photoresist pattern was transferred to the Ta mask via reactive ion beam etching, and after organic residue removal, SiN_x nano-cylinders were etched using SF_6/O_2 gas mixture (40/10 sccm) in a Lam 2300 KIYO system. The Ta mask and Al layer were removed using H_2SO_4/H_2O_2 mixture at 120°C for 15 minutes. High-resolution SEM was used to capture and analyze the distribution and dimensions of photoresist patterns and nanostructured pillars.

C. CHARACTERIZATION

The optical performance of the fabricated metalens is characterized using a broadband NKT SuperK white light laser, spectrally filtered by a 532 nm bandpass filter to isolate the green wavelength. The filtered beam undergoes beam expansion and an iris diaphragm to a diameter approximately half that of the metalens to ensure uniform illumination. To capture the focusing profile, a beam collection system comprising a 10× Plan APO broadband objective lens (NA = 0.26) and an M-LH-1A tube lens (focal length = 200 mm) was employed. The entire imaging system was mounted on a motorized translation stage for axial scanning. The intensity distribution at the focal plane and along the optical axis is recorded using a MicroPublisher 6^{TM} CCD scientific camera, with image acquisition and processing performed on a personal computer.

For quantitative assessment, the focusing and diffraction efficiencies were measured by first determining the incident beam power without the sample. The absolute focusing efficiency was then calculated as the ratio of the integrated optical power within six times the full width at half maximum (FWHM), corresponding to the detection area of our power meter, at the focal plane to the total incident power [32].

III. RESULTS AND DISCUSSION

We first evaluate the resist image prediction performance of the U-net and FCN models. The target nano-cylinder diameter, representing the desired critical dimension (CD), is compared with the predicted CD, which is extracted by approximating the nano-cylinder area as a perfect circle. Fig. 3(a) presents the average and worst-case ΔCD/CD errors (%) for U-net (red) and FCN (blue) over various training epochs. At 1500 epochs, the U-net model achieves optimal performance, with an average error of 0.2% and a worst-case error of 3.6%. In contrast, the FCN model yields an average error of 1.1% and a worst-case error of 8.0%. Extending training to 2000 epochs slightly improves FCN convergence but does not enhance U-net performance probably due to overfitting.

The error distribution at 1500 epochs is illustrated in Fig. 3(b), which shows a histogram of ΔCD/CD (%) across approximately 8,000 nano-cylinders in the validation dataset. The predictions of the U-net model are mostly within a 2% error margin, while the FCN model shows a broader distribution with average errors approaching 5%, indicating excellent fitting and convergence of the U-net model on this dataset.

Fig. 3(c) highlights the worst-case predictions from both models. The U-net output (bottom) closely resembles the target pattern, whereas the FCN prediction (top) shows noticeable deviations. A summary of the training and validation results at 1500 epochs, including average and worst ΔCD/CD values, is provided in Table 2.

TABLE 2. Model training result and generalization comparison.

Model	Val. loss	Val. accuracy	ΔCD/CD	
			Mean	Worst
FCN	0.8%	98.9%	1.1%	8.0%
U-net	0.4%	99.6%	0.2%	3.6%

We next evaluate the fabricated nano-pillar structures of the 2 mm-diameter metalenses after pattern transfer and etching processes. Figure 4(a) shows the top-view SEM image of the etched structures without any mask correction. Evidently, nano-cylinders with small feature sizes failed to stand upright, resulting in significant pillar collapse. Figures 4(b) and 4(c) show the etched results using mask corrections generated by the FCN and U-net models, respectively. In both cases, the smallest nano-cylinders with a feature size near the resolution limit remain well-resolved even when adjacent to large features, demonstrating the effectiveness of model-based mask correction in extending process latitude.

Figure 4(d) presents cross-sectional SEM images of the SiN_x pillars fabricated using the FCN-based OPC approach and the U-net-based IPC approach. Both small and large pillars exhibit measured heights of approximately 589nm,

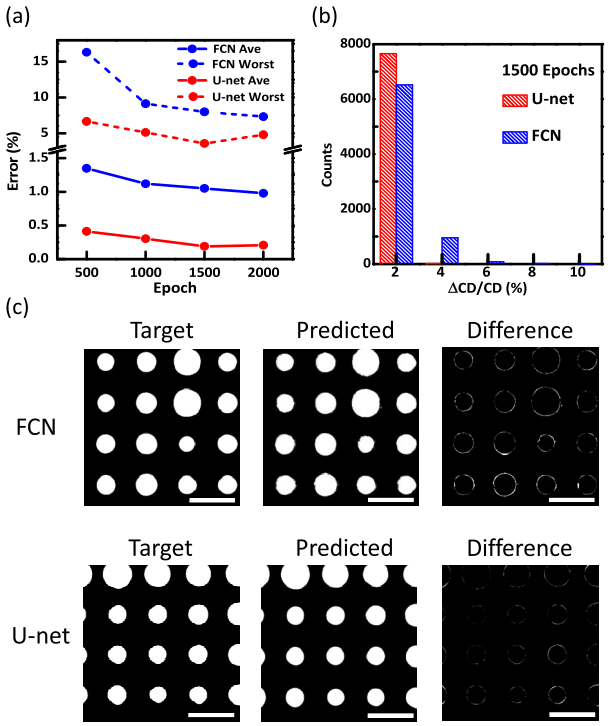

FIGURE 3. Prediction performance comparison between U-net and FCN lithographic models. (a) CD/CD error distributions across 1288 testing image pairs after 1500 training epochs. (b) Worst predictions with differences from target patterns for FCN (upper) and U-net (lower) models; scale: 1 μm. (c) Average and worst CD/CD errors versus training epochs.

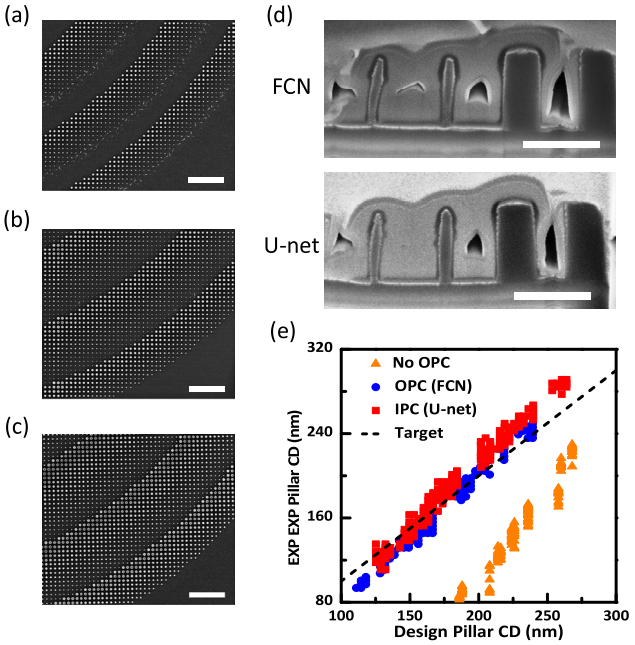

FIGURE 4. Top-view SEM images of the 2mm-diameter metalens patterns: (a) Non-OPC result, showing significant collapse of small-feature pillars; (b) OPC approach with the FCN model; and (c) IPC approach with the U-net model. All scale bars: 4μm. (d) Cross-sectional SEM images of the largest and smallest SiN_x nano-cylinders fabricated with OPC (FCN) approach (top), and IPC (U-net) approach (bottom), showing consistent heights and demonstrating enhanced process latitude in a single exposure. Scale bar: 600nm. (e) Correlation analysis between designed and experimentally measured critical dimensions (CDs) of nano-cylinders, comparing non-OPC, OPC, and IPC approaches.

closely matching the designed height of 585nm and the smallest pillar achieves an aspect ratio approaching 1:6. We have evaluated nanocolumn stability within the entire metasurface region. Before OPC, the collapse rate of nanocolumns was 34.5%; after applying the IPC, the collapse rate was reduced to 0%, demonstrating a substantial improvement in structural yield.

Figure 4(e) analyzes the correlation between the designed and experimentally measured CDs of the nano-cylinders. In the non-OPC case, a steep slope ∼1.7 indicates poor CD control, such that small features are not resolved. In contrast, both OPC and IPC layouts demonstrate improved CD linearity, with slope values approaching unity (∼1.1). However, process variations in etching and pattern transfer results in CD deviations from the target values (dashed line). Overall, the average CD distribution in the OPC layout (blue dots, Fig. 4(e)) closely matches the target values, with less than 10 nm deviation for small features. The IPC layout also follows the target closely (red squares, Fig. 4(e)) with slightly larger deviations for the large pillars. These results demonstrate that the IPC approach achieves excellent CD control comparable to the OPC, enhancing the fidelity of metalens fabrication.

The focusing characteristics of three 2mm-diameter metalenses with 0.1 NA are presented in Fig.5: (a) without OPC, (b) with OPC using the FCN model, and (c) with IPC using the U-net model. For each case, the focusing spot, axial intensity profile, and corresponding modulation transfer function (MTF) are shown from left to right, respectively. All three metalenses exhibit clear focusing behavior with a measured focal length of approximately 10.0 mm, closely matching the design specification of 9.9 mm. Although the non-OPC metalens shows substantial CD deviations and fails to resolve small features due to proximity effects, it still retains basic focusing capability. However, the focal spot size is significantly larger than those achieved with model-based corrections, and its absolute focusing efficiency is considerably lower.

The focal spot sizes, determined by the FWHM, are measured to be approximately 5.3 μm for both OPC (FCN) and IPC (U-net) metalenses which closely match the theoretical diffraction-limited value of 4.6 μm. In contrast, the non-OPC metalens exhibits a significantly larger FWHM of ∼7.1 μm, highlighting the strong correlation between pattern fidelity and optical performance. The performance improvement with photomask correction is further supported by the modulation transfer function (MTF) analysis. The calculated Strehl ratios—defined as the ratio of the integrated area under the measured MTF to that of the ideal diffraction-limited MTF—are 0.64 for the non-OPC, 0.95 for the OPC, and 0.93 for the

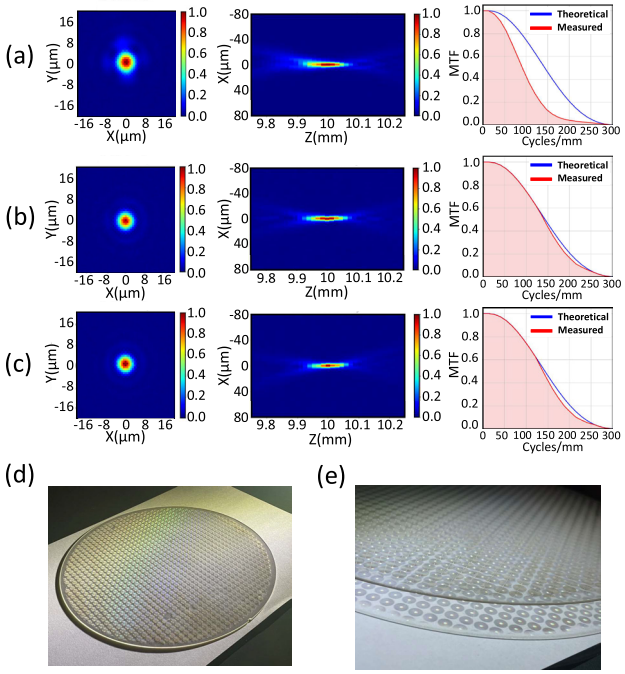

FIGURE 5. The Focusing performance of 2 mm-diameter metalenses: (a) without OPC, (b) with OPC (FCN), and (c) with IPC (U-net), showing 2D focal spot (left), axial profile (center), and MTF (right; red: measured, blue: theoretical). (d) Photograph of 4.5 mm IPC metalenses on an 8-inch wafer. (e) Close-up view showing focal spots under white light illumination.

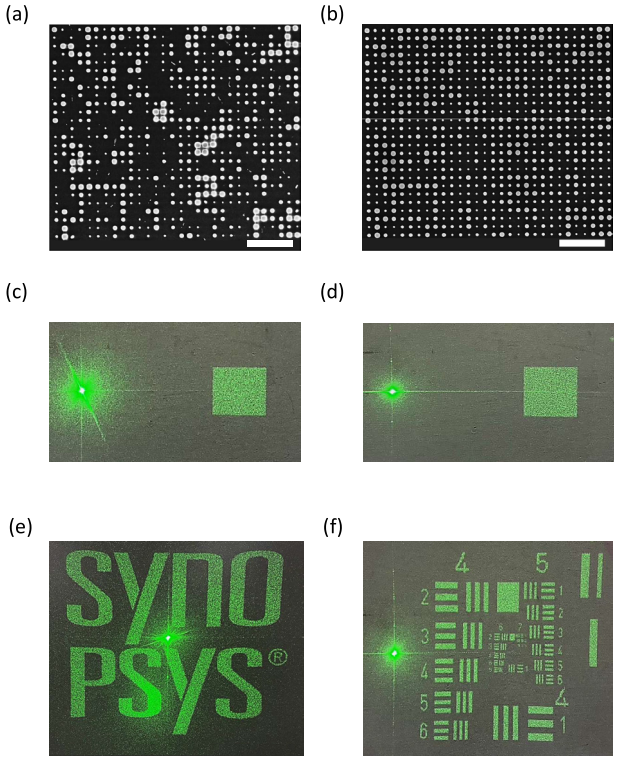

FIGURE 6. Top-view SEM images of SiN_x nano-cylinders on (a) non-OPC MOE and (b) IPC MOE devices. Scales are 4μm.The corresponding reconstructed pattern in the far field from (a) and (b) are shown in (c) and (d), respectively. (e) and (f) show photographs of customized patterns from IPC metasurface hologram under green light (532nm) excitation.

IPC metalens. These results indicate that both OPC and IPC enable near-diffraction-limited imaging performance, with the IPC approach showing comparable optical quality to the OPC method.

In terms of focusing efficiency, the non-OPC metalens achieves 42.7 $\pm$ 4.2%, while the OPC and IPC metalenses reach 51.9 $\pm$ 0.8% and 50.6 $\pm$ 2.0%, respectively, averaged over three devices per case. These measurements confirm that CD errors in the non-OPC design introduce optical aberrations and reduce both resolution and optical throughput. In contrast, model-based OPC and IPC approaches effectively suppress the CD errors, yielding higher focusing efficiency. Notably, the OPC metalens benefits from its explicit use of the optical model, exhibiting slightly higher average efficiency and smaller standard deviation than IPC. Nevertheless, the IPC approach, enabled by the U-net model, offers key advantages in terms of model transferability and computational scalability. As an end-to-end learning-based solution that does not require complex aerial image simulations, IPC is more adaptable to different CMOS process nodes and lithographic conditions.

Scaling the metalens diameter from the millimeter to centimeter results in an exploded number of nano-cylinders to over billions, posing a significant computational burden for the model based OPC approach. Moreover, the mask data size will also be significantly increased, and currently surpass the capacity our mask shop could handle with a laser beam reticle writer. In terms of computing time, the IPC (U-net) takes 2 hours 25 min. for correcting a 2mm diameter metalens with MPI, which is ~3 times faster than the OPC (FCN) approach and ~35 times faster than the OPC without MPI. Since IPC metalens can obtain comparable performance to the OPC metalens, we further design and fabricate 4.5 mm diameter metalenses on full 8-inch glass wafer, producing over 1000 pieces of high quality metalenses in a single photolithographic step (Fig. 5(d) and 5(e)).

The optical characterization of IPC-corrected metalenses underscores the importance of pattern fidelity in achieving the intended optical performance. To further demonstrate the versatility of the IPC system, we extend its application beyond regular patterns such as metalenses to more complex, randomly distributed metasurface holograms. Specifically, we design 1.5 $\times$ 1.5 mm^2 metasurface holograms that generate customized far-field diffraction patterns. Partial SEM images of the fabricated devices are shown in Fig. 6(a) for the non-IPC case and Fig. 6(b) for the IPC-corrected case. The IPC approach successfully resolves nanoscale features, particularly small-diameter nano-cylinders, while the non-IPC sample exhibits significant CD variation and loss of resolution. The designed far-field diffraction pattern is a rectangular shape which is intentionally deflected by 10° from the optical axis to spatially separate it from the DC component caused by unmodulated light.

Figure 6(c) displays the reconstructed far-field pattern from the non-IPC device, showing pronounced speckle and

noise near the DC region. In contrast, the IPC-corrected device (Fig. 6(d)) exhibits a much cleaner reconstruction with reduced speckle intensity. These results indicate that while metasurface holograms are relatively tolerant to phase errors, unresolved features in the non-IPC sample contribute to an amplified DC component, degrading beam-shaping performance. Figures 6(e) and 6(f) show the photographs of the customized diffraction patterns produced by the fabricated metasurface holograms. Notably, the IPC-corrected device resolves the tri-bar structure in element 3, group 7, which corresponds to the line-space resolution limit on the design target. This result demonstrates the robustness and fidelity of the metasurface design and fabrication with the proposed IPC system.

Finally, while this work demonstrates wafer-scale fabrication of 4.5 mm diameter metalenses and metasurface holograms, the extension to centimeter-scale devices is currently limited by the file-handling capacity of our mask shop, not by the IPC algorithm itself, which already leverages parallel computing. We also acknowledge that the end-to-end U-net surrogate lacks the interpretability of physics-based OPC methods, making it less straightforward to diagnose failure modes or tune process variations. Nevertheless, the U-net model effectively reproduces the optics of our prior FCN model, delivering nearly identical pattern fidelity with substantially faster convergence. For metasurfaces with limited pattern diversity, such as those on fixed lattices, the risk of encountering unseen geometries is low, making the U-net model approach both robust and practical. In these cases, speed and simplicity are highly advantageous, allowing deployment in laboratories or foundries without reliance on costly EDA toolchains. Looking ahead, hybrid frameworks that embed physics-based constraints or uncertainty quantification into the neural-network pipeline could provide a balance between interpretability and computational efficiency, extending applicability to complex metasurface patterning.

IV. CONCLUSION

In this work, we introduce an intelligent proximity correction (IPC) system to facilitate scalable metasurface fabrication by KrF photolithography. By combining a deep learning lithographic model with efficient parallel computing strategies, the IPC overcomes the speed and accuracy limitations of the traditional OPC method. This approach enables the realization of large-area, high-efficiency metasurfaces using economical photolithography techniques, opening new possibilities in the field of flat optics and nano-photonics. Furthermore, the IPC system highlights an end to end modeling technique without involving complex optical image calculations. Therefore, the IPC system can be easily adapted or transferred to different lithography processes, showing its potential to accelerate the development of next-generation optical and semiconductor devices through cost-effective, high-throughput manufacturing.

ACKNOWLEDGMENT

The authors would like to thank the National Center for High-performance Computing (NCHC), National Institutes of Applied Research, Taiwan, for computational and storage resources. They also acknowledge Mr. Richard L. C. Hu, and Dr. Chenglin Xu, at Synopsys Inc. for their valuable discussions and technical support.

REFERENCES

[1] N. Yu and F. Capasso, "Flat optics with designer metasurfaces," *Nature Mater.*, vol. 13, no. 2, pp. 139–150, Feb. 2014, doi: 10.1038/nmat3839.

[2] S. Jahani and Z. Jacob, "All-dielectric metamaterials," *Nature Nanotechnol.*, vol. 11, no. 1, pp. 23–36, Jan. 2016, doi: 10.1038/nnano.2015.304.

[3] J. Hu, S. Bandyopadhyay, Y.-H. Liu, and L.-Y. Shao, "A review on metasurface: From principle to smart metadevices," *Frontiers Phys.*, vol. 8, Jan. 2021, Art. no. 586087, doi: 10.3389/fphy.2020.586087.

[4] M. K. Chen, Y. Wu, L. Feng, Q. Fan, M. Lu, T. Xu, and D. P. Tsai, "Principles, functions, and applications of optical meta-lens," *Adv. Opt. Mater.*, vol. 9, no. 4, Feb. 2021, Art. no. 2001414, doi: 10.1002/adom.202001414.

[5] A. Arbabi and A. Faraon, "Advances in optical metalenses," *Nature Photon.*, vol. 17, no. 1, pp. 16–25, Jan. 2023, doi: 10.1038/s41566-022-01108-6.

[6] A. She, S. Zhang, S. Shian, D. R. Clarke, and F. Capasso, "Large area metalenses: Design, characterization, and mass manufacturing," *Opt. Exp.*, vol. 26, no. 2, pp. 1573–1585, 2018, doi: 10.1364/oe.26.001573.

[7] S. Colburn, A. Zhan, and A. Majumdar, "Varifocal zoom imaging with large area focal length adjustable metalenses," *Optica*, vol. 5, no. 7, pp. 825–831, 2018, doi: 10.1364/optica.5.000825.

[8] H. Cheng, Z. Tang, L. Wu, C. Peng, and J. Sun, "CMOS-compatible A—Si metalenses on a 12-inch glass wafer for fingerprint imaging," *Nature Commun.*, vol. 13, no. 1, pp. 4789–4796, 2022, doi: 10.1515/nanoph-2019-0470.

[9] Y. Yang, K. Kelley, J. D. B. Yao, and F. Capasso, "All-glass, large metalens at visible wavelength using deep-ultraviolet projection lithography," *Nature Commun.*, vol. 11, no. 1, pp. 2300–2310, 2020, doi: 10.1021/acs.nanolett.9b03333.

[10] P. Yu, "True process variation aware optical proximity correction with variational lithography modeling and model calibration," *J. Micro/Nanolithography, MEMS, MOEMS*, vol. 6, no. 3, Jul. 2007, Art. no. 031004, doi: 10.1117/1.2752814.

[11] S. Palatnick, D. John, and M. Millar-Blanchaer, "Investigating pathways for deep-UV photolithography of large-area nanopost-based metasurfaces with high feature-size contrast," *J. Vac. Sci. Technol. B*, vol. 42, no. 6, Dec. 2024, Art. no. 062602, doi: 10.1116/6.0003947.

[12] N. B. Cobb, A. Zakhor, and E. A. Miloslavsky, "Mathematical and CAD framework for proximity correction," *Proc. SPIE*, vol. 2726, pp. 208–222, Jun. 1996, doi: 10.1117/12.240907.

[13] X. Ma, Z. Wang, Y. Li, G. R. Arce, L. Dong, and J. Garcia-Frias, "Fast optical proximity correction method based on nonlinear compressive sensing," *Opt. Exp.*, vol. 26, no. 11, pp. 14479–14498, 2018, doi: 10.1364/oe.26.014479.

[14] N. Cobb, "Fast optical and process proximity correction algorithms for integrated circuit manufacturing," Ph.D. dissertation, Dept. Elect. Eng. and Comput. Sci., Univ. of California, Berkeley, CA, USA, 1998.

[15] X. Ma and G. R. Arce, "Pixel-based OPC optimization based on conjugate gradients," *Opt. Exp.*, vol. 19, no. 3, pp. 2165–2180, 2011, doi: 10.1364/oe.19.002165.

[16] Y. Lin, Y. Watanabe, T. Kimura, T. Matsunawa, S. Nojima, M. Li, and D. Z. Pan, "Data efficient lithography modeling with residual neural networks and transfer learning," in *Proc. Int. Symp. Phys. Design*, Mar. 2018, pp. 82–89, doi: 10.1145/3177540.3178242.

[17] H.-C. Shao, C.-Y. Peng, J.-R. Wu, C.-W. Lin, S.-Y. Fang, P.-Y. Tsai, and Y.-H. Liu, "From IC layout to die photograph: A CNN-based data-driven approach," *IEEE Trans. Comput.-Aided Design Integr. Circuits Syst.*, vol. 40, no. 5, pp. 957–970, May 2021, doi: 10.1109/TCAD.2020.3015469.

[18] A. Lin, T. Rawat, C.-Y. Chang, H.-C. Tung, H.-L. Liu, and P. Yu, "Optical proximity correction using machine learning assisted human decision," *IEEE Photon. J.*, vol. 15, no. 1, pp. 1–9, Feb. 2023, doi: 10.1109/JPHOT.2022.3231426.

[19] D. Gostimirovic, Y. Grinberg, D.-X. Xu, and O. Liboiron-Ladouceur, "Improving fabrication fidelity of integrated nanophotonic devices using deep learning," *ACS Photon.*, vol. 10, no. 6, pp. 1953–1961, Jun. 2023, doi: 10.1021/acsphotonics.3c00389.
[20] V. Joshi, M. Le Gallo, S. Haefeli, I. Boybat, S. R. Nandakumar, C. Piveteau, M. Dazzi, B. Rajendran, A. Sebastian, and E. Eleftheriou, "Accurate deep neural network inference using computational phase-change memory," *Nature Commun.*, vol. 11, no. 1, p. 2473, May 2020, doi: 10.1038/s41467-020-16108-9.
[21] X. Zheng, X. Ma, Q. Zhao, Y. Pan, and G. R. Arce, "Model-informed deep learning for computational lithography with partially coherent illumination," *Opt. Exp.*, vol. 28, no. 26, pp. 39475–39491, Dec. 2020, doi: 10.1364/oe.413721.
[22] D. Gostimirovic, D.-X. Xu, O. Liboiron-Ladouceur, and Y. Grinberg, "Deep learning-based prediction of fabrication-process-induced structural variations in nanophotonic devices," *ACS Photon.*, vol. 9, no. 8, pp. 2623–2633, Aug. 2022, doi: 10.1021/acsphotonics.1c01973.
[23] R. Zhao, Y. Wei, X. Wang, X. He, and H. Xu, "Convolutional neural network-assisted photoresist formulation discriminator design of a contact layer for electron beam lithography," *J. Phys. Chem. Lett.*, vol. 15, no. 34, pp. 8715–8720, Aug. 2024, doi: 10.1021/acs.jpclett.4c01911.
[24] W.-P. Liao, H.-L. Liu, Y.-F. Lin, S.-S. Su, Y.-T. Chen, G.-B. Lin, T.-C. Tseng, T.-K. Lin, C.-C. Chen, W.-H. Huang, S.-W. Chen, J.-M. Shieh, P. Yu, and Y.-C. Chang, "I-line photolithographic metalenses enabled by distributed optical proximity correction with a deep-learning model," *Opt. Exp.*, vol. 30, no. 12, pp. 21184–21194, 2022, doi: 10.1364/oe.456469.
[25] O. Ronneberger, P. Fischer, and T. Brox, "U-Net: Convolutional networks for biomedical image segmentation," in *Proc. Med. Image Comput. Comput.-Assist. Intervent.*, 2015, pp. 234–241, doi: 10.1007/978-3-319-24574-4_28.
[26] J. S. Suri, M. Bhagawati, S. Agarwal, S. Paul, A. Pandey, S. K. Gupta, L. Saba, K. I. Paraskevas, N. N. Khanna, J. R. Laird, A. M. Johri, M. K. Kalra, M. M. Fouda, M. Fatemi, and S. Naidu, "UNet deep learning architecture for segmentation of vascular and non-vascular images: A microscopic look at UNet components buffered with pruning, explainable artificial intelligence, and bias," *IEEE Access*, vol. 11, pp. 595–645, 2023, doi: 10.1109/ACCESS.2022.3232561.
[27] A. Zhan, S. Colburn, R. Trivedi, T. K. Fryett, C. M. Dodson, and A. Majumdar, "Low-contrast dielectric metasurface optics," *ACS Photon.*, vol. 3, no. 2, pp. 209–214, Feb. 2016, doi: 10.1021/acsphotonics.5b00660.
[28] Z. Lin and S. G. Johnson, "Overlapping domains for topology optimization of large-area metasurfaces," *Opt. Exp.*, vol. 27, no. 22, pp. 32445–32453, Oct. 2019, doi: 10.1364/oe.27.032445.
[29] V. Kettunen, "Review of iterative Fourier-transform algorithms for beam shaping applications," *Opt. Eng.*, vol. 43, no. 11, pp. 2549–2556, Nov. 2004, doi: 10.1117/1.1804543.
[30] Y. Wu, J. Wang, C. Chen, C.-J. Liu, F.-M. Jin, and N. Chen, "Adaptive weighted gerchberg-saxton algorithm for generation of phase-only hologram with artifacts suppression," *Opt. Exp.*, vol. 29, no. 2, p. 1412, 2021, doi: 10.1364/oe.413723.
[31] S. Liu and Y. Takaki, "Optimization of phase-only computer-generated holograms based on the gradient descent method," *Appl. Sci.*, vol. 10, no. 12, p. 4283, Jun. 2020, doi: 10.3390/app10124283.
[32] M. Khorasaninejad, A. Y. Zhu, C. Roques-Carmes, W. T. Chen, J. Oh, I. Mishra, R. C. Devlin, and F. Capasso, "Polarization-insensitive metalenses at visible wavelengths," *Nano Lett.*, vol. 16, no. 11, pp. 7229–7234, Nov. 2016, doi: 10.1021/acs.nanolett.6b03626.

HSUEH-LI LIU received the bachelor's degree in photonics from National Yang Ming Chiao Tung University, in 2019, where he is currently pursuing the Ph.D. degree. His research focuses on metasurface optics, photolithography, optical proximity correction (OPC), and the application of deep neural networks for lithography modeling and computational acceleration. In particular, he explores data-driven techniques for layout-to-image prediction and OPC mask optimization using deep-learning models. He is a Student Member of SPIE and has received multiple research awards in Taiwan.

SHENG-HSIANG SU received the M.S. degree in photonics from National Yang Ming Chiao Tung University, Taiwan, in 2022. He published his work through SPIE and was a SPIE Student Member during his graduate studies. In the same year, he joined the OPC mask correction development division with Taiwan Semiconductor Manufacturing Company (TSMC) as a Lithography Engineer, working on inverse lithography correction and AI-based lithography modeling. His research focused on resolution enhancement techniques, intelligent proximity correction, and AI-based lithography modeling.

PO-KAI CHANG is currently pursuing the Ph.D. degree with National Yang Ming Chiao Tung University. His research focuses on computational lithography and metasurfaces. He works on optimizing lithography techniques through numerical simulations and explores the applications and fabrication processes of metasurfaces in optical components, offering innovative solutions for semiconductor processes and optical technologies. He has been a SPIE Student Member, since 2024.

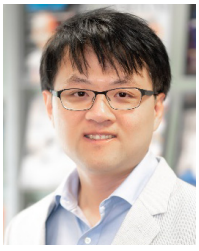

YOU-CHIA CHANG was born in Taichung, Taiwan, in 1981. He received the Ph.D. degree in applied physics from the University of Michigan, in 2016. From 2016 to 2018, he was a Postdoctoral Research Scientist with the Department of Electrical Engineering, Columbia University, New York, USA. In 2018, he joined the Department of Photonics, National Yang Ming Chiao Tung University, Hsinchu, Taiwan, where he is currently an Associate Professor. His research interests include silicon photonics metamaterials/metasurfaces, and two-dimensional materials. He was a recipient of the Jade Mountain (Yushan) Young Scholar Award.

YAO-WEI HUANG (Member, IEEE) received the Ph.D. degree in applied physics from National Taiwan University, with expertise spanning nanophotonics, materials science, nanofabrication, and nanotechnology. He is currently an Associate Professor of photonics and a Yushan Young Scholar with National Yang Ming Chiao Tung University (NYCU). He has extensive research experience from prestigious institutions, such as Harvard, Caltech, and NUS. His research focuses on cutting-edge topics, such as nanophotonics, metasurfaces, meta-optics, inverse design, nonlocal effects, structured light, dispersion engineering, and computational visual sensing, with innovative applications in extended reality and depth perception. His work aims to advance metasurface technologies to benefit human well-being. He is also a fellow of the Higher Education Academy (HEA) and a SPIE Senior Member. He received the Dean's Award from National Taiwan University, during his Ph.D. studies.

CHIA-WEI CHANG received the B.S. degree in photonics from Feng Chia University, Taichung, Taiwan. He is currently pursuing the M.S. degree in electro-optical engineering with National Yang Ming Chiao Tung University, Hsinchu, Taiwan. He has worked with United Microelectronics Corporation, Hsinchu, and Giga Solution Tech. Company Ltd., Hsinchu. He is currently with the Taiwan Semiconductor Research Institute, Hsinchu. His research interests include MEEF and OPC modeling, lithography process optimization, and metasurface-based optical system design.

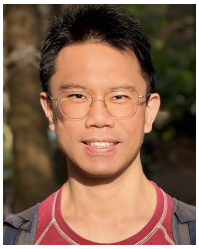

TSAI-MING HUANG received the M.S. degree in materials science and engineering from National Tsing Hua University, Taiwan, in 2000. He was with TSMC, from 2011 to 2020, on advanced lithography for embedded flash and MRAM. He is currently a Lithography Process Engineer with Taiwan Semiconductor Research Institute, National Institute of Applied Research (TSRI/NIAR), focusing on DUV lithography, OPC, and novel channel materials.

CHUN-CHI CHEN received the B.S. and M.S. degrees in atomic science from National Tsing Hua University, Taiwan, in 1998 and 2000, respectively, and the Ph.D. degree in materials science and engineering from National Yang Ming Chiao Tung University, Taiwan, in 2013. Since 2018, he has been with Taiwan Semiconductor Research Institute (TSRI), National Applied Research Laboratories, where he serves as the Group Leader of the Photomask Lithography Team. His research interests include photoresist materials, exposure systems, lithography process development, and resolution enhancement technologies.

WEN-HSIEN HUANG received the Ph.D. degree in materials science and engineering from National Yang Ming Chiao Tung University, Taiwan. He is a Research Fellow and the Division Director of semiconductor thin-film deposition and etch modules with Taiwan Semiconductor Research Institute (TSRI), National Institutes of Applied Research. His research focuses on low thermal budget technologies for semiconductor materials and devices, including plasma Si/Ge/SiGe thin-film deposition, laser crystallization and laser dopant activation, which are widely employed in applications of Si-based monolithic 3DIC, glass-based TFT and flexible transistors. Furthermore, his recent research extends to GaN epitaxy and high-frequency GaN-HEMT fabrication.

JIA-MIN SHIEH received the Ph.D. degree in electro-optics from National Yang Ming Chiao Tung University, Taiwan, in 1997. In 1998, he joined National Nano Device Laboratories (NDL), Taiwan, and became a Researcher, in 2003. Currently, he is a Senior Research Fellow with TSRI (former NDL). His academic interests include flexible electronics, advanced CIM memories, and heterogeneously integrated 3D ICs. His team is engaged in developing flexible electronics, low-cost TSV-free monolithic 3D-ICs, energy-saving MEMS sensors, and advanced memory technology.

PEICHEN YU (Member, IEEE) received the Ph.D. degree in electrical engineering from the University of Michigan, Ann Arbor, MI, USA, in 2004. From 2004 to 2006, she joined the Advanced Design Group, Intel Corporation, Hillsboro, OR, USA, as a Resolution Enhancement Technology (RET) Design Engineer. Since 2006, she switched careers to academia and is currently a Professor with the Department of Photonics, National Yang Ming Chiao Tung University. Her research interests include nanostructures and metasurfaces patterning for optoelectronic applications. She is also actively engaged in the development of RET solutions, including inverse lithography technology (ILT) for ArF 193i and EUV lithography. She has published over 60 refereed technical articles in the above research areas. Her work has been highlighted in various scientific journals, including Virtual Journal of Nanoscale Science and Technology, SPIE Newsroom, and NPG Nature Asia-Material. She is also a member of the IEEE Photonics Society and SPIE. She received several research and teaching awards in Taiwan.